



Contents lists available at SciVerse ScienceDirect

# Journal of Quantitative Spectroscopy & Radiative Transfer

journal homepage: [www.elsevier.com/locate/jqsrt](http://www.elsevier.com/locate/jqsrt)



## Climatological aspects of aerosol optical properties in North China Plain based on ground and satellite remote-sensing data



Xiangao Xia <sup>a,\*</sup>, Hongbin Chen <sup>a</sup>, Philippe Goloub <sup>b</sup>, Xuemei Zong <sup>a</sup>,  
Wenxing Zhang <sup>a</sup>, Pucai Wang <sup>a</sup>

<sup>a</sup> LAGEO, Institute of Atmospheric Physics, Chinese Academy of Sciences, Beijing, China

<sup>b</sup> LOA (Laboratoire d'Optique Atmosphérique), Université Lille, Lille, France

### ARTICLE INFO

#### Article history:

Received 17 May 2013

Received in revised form

25 June 2013

Accepted 26 June 2013

Available online 5 July 2013

#### Keywords:

Aerosol optical properties

AERONET

MODIS

CALIOP

NCP

### ABSTRACT

Aerosol data from the Aerosol Robotic Network (AERONET), Moderate Resolution Imaging Spectroradiometer (MODIS), and Cloud–Aerosol Lidar with Orthogonal Polarization (CALIOP) recorded during the new millennium were used to investigate the spatio-temporal variation of aerosol optical properties in the North China Plain (114–120°E; 34.5–41°N). The external linear mixing of both fine and coarse mode components dominated variations of the refractive index and the single scattering albedo ( $\omega$ ) in spring and winter when the fine mode fraction (FMF) was  $<0.6\text{--}0.7$ . The effective radius of fine mode component increased rapidly with FMF in every season when FMF exceeded  $\sim0.6\text{--}0.7$ , and thereby when  $\omega$  increased significantly. With the exception of dust cases, aerosols resembled the mixed category in every season except summer; summer aerosols resembled the industry/urban category. The aerosol layer height was observed to be 2–3 km in summer; however, aerosols were trapped below 1–2 km in fall and winter. Aerosol optical depth (AOD) retrieved by the MODIS was in good agreement with the AERONET AOD ( $R > 0.80$ ). The MODIS tended to overestimate AOD in spring and summer. This feature was most prominent at 660 nm; therefore, MODIS Ångström exponents were poorly derived. A strong correlation ( $R > 0.7$ ) between the AERONET AODs in Beijing and the MODIS level 2.0 pixel AODs persisted for a large and strongly anisotropic area of  $\sim 17,000 \text{ km}^2$  in winter to  $\sim 100,000 \text{ km}^2$  in fall, indicating that the aerosol pollution is regional in nature. A decreasing trend was derived for the AERONET and MODIS AOD data, although no trends were significant. Further understanding of the seasonal variations of aerosol optical properties in this polluted region would help to improve satellite aerosol retrieval and to promote regional climate change research.

© 2013 Elsevier Ltd. All rights reserved.

## 1. Introduction

The climate is a complex system controlled by the energy budget of Earth. Aerosols interact with the Earth's energy balance through the scattering and absorption of sunlight [1]. Indirectly, aerosols have a substantial effect on cloud properties and the initiation of precipitation [2] (and references therein). Much of the uncertainty in climate modeling and projections of climate change is

due to the complexity of aerosols. To identify and quantify the uncertainty in radiative forcing and climate change, observation of the physical and optical properties of aerosols and their radiative and climatic impacts is urgently required, particularly over polluted regions.

The North China Plain (NCP; 114–120°E, 34.5–41°N) is based on the deposits of the Yellow River and is the largest alluvial plain of eastern Asia. The plain is bordered to the north by the Yanshan Mountains and to the west by the Taihang Mountains at the edge of the Loess Plateau. To the south, it merges into the Yangtze Plain. From northeast to southeast, the plain fronts the Bohai Sea, the highlands of

\* Corresponding author. Tel.: +86 108 299 5071; fax: +86 108 299 5073.  
E-mail address: [xxa@mail.iap.ac.cn](mailto:xxa@mail.iap.ac.cn) (X. Xia).

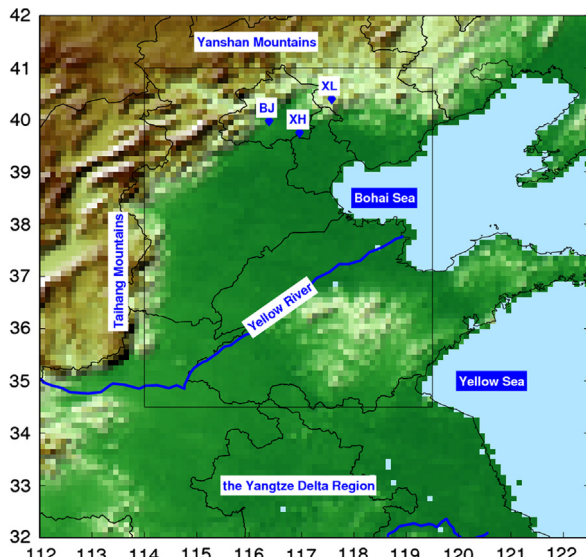


**Fig. 1.** Topography of North China Plain (NCP) and the three representative AERONET stations including Beijing—urban: 116.92, 39.75; Xianghe—suburban: 116.38, 39.98; and Xinglong—background: 117.58, 40.39.

Shandong Peninsula, and the Yellow Sea (Fig. 1). The NCP is a densely populated region in China and has experienced unprecedented economic and population growth during the past three decades, which has resulted in a general decline in air quality [3–5]. The mixture of coarse dust particles with heavy anthropogenic pollution created by industrial and agricultural activities and urbanization has resulted in a rather complex nature of aerosol physical and optical properties [6,7].

To monitor the long-term changes in atmospheric components at a regional scale, three Aerosol Robotic Network (AERONET) stations were established in urban, suburban, and background areas of the NCP (Fig. 1). These AERONET data were widely used to characterize aerosol optical properties [8], to validate satellite retrievals [9,10], to study aerosol radiative forcing [11,12], and to reveal regional air pollution episodes [13,14]. The Moderate Resolution Imaging Spectroradiometer (MODIS), which was deployed on the Terra and Aqua satellites in early 2000 and mid-2002, respectively, has retrieved aerosol optical depth (AOD) with 20% accuracy over land [15], and its aerosol data has provided regional and global views of the aerosol system. The MODIS aerosol product has been widely used in geophysical applications such as studies of regional and seasonal distributions of major aerosol systems [16,17], intercontinental transportation of pollutants [18], and aerosol–cloud interaction [19]. In addition, its product has been used to determine and quantify aerosol source strength [20]. Cloud–Aerosol Lidar with Orthogonal Polarization (CALIOP) is the primary instrument of the Cloud–Aerosol Lidar and Infrared Pathfinder Satellite Observation (CALIPSO) satellite launched in mid-2006. CALIOP was designed to provide a global 3-D view of aerosols and clouds and is expected to improve the performance of a variety of atmospheric models ranging from global climate to small-scale cloud resolving models [21] (and references therein).

The objective of this study is to present a 4-D view of aerosol optical properties in the NCP by using AERONET, MODIS, and CALIPSO data. The variability of aerosol optical properties on various spatial and time scales is shown in this paper.

## 2. Ground and satellite remote sensing aerosol data

### 2.1. Ground sunphotometer data

In spring of 2001, two Cimel sunphotometers were installed temporarily in Beijing and Xianghe, as part of the Aerosol Characterization Experiment–Asia project (ACE–Asia). Three permanent AERONET sites were established in the NCP. The first two locations were in Beijing and Xianghe in April 2002 and August 2004, respectively. In February 2006, the third AERONET site was established at the top of a mountain (970 m a.s.l.) in Xinglong at a regional background station. A long-term, continuous, and readily accessible public domain database of aerosol optical, microphysical, and radiative properties recorded at these three stations are downloaded from the AERONET website (<http://aeronet.gsfc.nasa.gov>). The measurement and calibration protocol, processing algorithm, and data quality have been detailed in previous research [22,23]. Table 1 shows the observation period at these 3 AERONET stations.

### 2.2. MODIS data

MODIS was deployed on Terra and Aqua satellites launched in December 1999 and May 2002, respectively. The MODIS aerosol retrieval algorithm over land has been improved periodically and has been designated by various collections since its initial launch [15]. The MODIS dark-target AOD data have evolved to the Collection 5.1 that is used in this study. Validation at more than 30 sites across China showed that the correlation coefficient between MODIS and ground-based AODs was 0.84. The offset and the slope was 0.047 and 0.98, respectively [9]. We used the Level 2.0 MODIS AOD data, which have a spatial resolution of 10 km at nadir. The Level 2 MODIS aerosol products also contain retrieval quality assurance (QA). Only QA3 (high confidence) data were used in the analysis. The data since March 2000 from Terra and July 2002 from Aqua were downloaded from the GSFC LAADS web (<http://ladsweb.nascom.nasa.gov>).

### 2.3. CALIOP data

CALIOP is the primary instrument on the CALIPSO satellite. Its main function is to acquire vertical profiles of elastic backscatter at 532 nm and 1064 nm from a near

**Table 1**  
AERONET data at Beijing, Xianghe and Xinglong.

Station	Observation period	Number of month
BJ	2001/03–2001/05; 2004/04–2012/08	123
XH	2001/04–2001/05; 2005/09–2012/06	94
XL	2006/02–2012/09	57

nadir-viewing geometry during both day and night phases of the orbit. The primary products are three calibrated and geolocated lidar profiles including a 532 nm and 1064 nm total attenuated backscatter and a 532 nm perpendicular polarization component with variable vertical and horizontal resolutions [21]. The CALIOP version 3 level 2532 nm aerosol extinction data recorded from July 2006 to October 2011 used in this study were obtained from the CALIPSO website (<http://www-calipso.larc.nasa.gov>). The vertical resolution of the data is 60 m, from  $-0.5$  to 12 km. Monthly mean extinction profiles were calculated for all aerosol species under nighttime all-sky conditions. Results of the aerosol type classification contained in Level 2 aerosol products were used to calculate the monthly occurrence of frequency of five major aerosol types including, dust, polluted dust, smoke, polluted continental, and clear continental. Detailed information on aerosol type classification has been described by Omar et al. [24].

### 3. Seasonal variation of aerosol properties

#### 3.1. Seasonal aspects of aerosol optical properties of fine/coarse aerosol mixtures

Previous research has indicated that the single scattering albedo ( $\omega$ ) varied linearly with the fine mode fraction (FMF) at Beijing in spring when  $FMF < \sim 0.7$  [8]. This finding indicates that variation in  $\omega$  is dominated by

external linear mixing of both fine and coarse mode components, of which  $\omega$  remains relatively constant for this range of FMF. Fig. 2 presents analysis of FMF and  $\omega$  in spring, March–May; summer, June–August; fall, September–November; and winter, December–February. The color bar indicates the effective radius of the fine mode component ( $RE_f$ ). This analysis was extended to the real and imaginary part of the refractive index (Fig. 3).  $\omega$  at every wavelength except 440 nm decreased linearly with FMF when FMF was  $< \sim 0.6$  in spring and  $< \sim 0.7$  in winter. This linear decrease in  $\omega$  as a function of FMF is not attributed to particle size because  $RE_f$  remained constant within this range of FMF ( $\sim 0.15$ ). Eck et al. suggested that this phenomenon is likely the result of increased absorption of fine mode components in a system with a linear mixture of fine and coarse components or coating of coarse mode particles [8]. This suggestion has been supported by observation of the imaginary part of the refractive index increasing linearly with FMF. Absorbing aerosol components in the visible range include black carbon (BC) and brown carbon (BrC). BC absorption shows little wavelength dependence; however, BrC absorption decreases with wavelength. BC was likely the dominant absorbing component because the imaginary part at every wavelength except 440 nm increased with FMF at the same rate.  $\omega_{440\text{ nm}}$  remained relatively stable when FMF was  $< \sim 0.6$ –0.7. However, the imaginary part of refractive index increased and the real part decreased with FMF (Fig. 2),

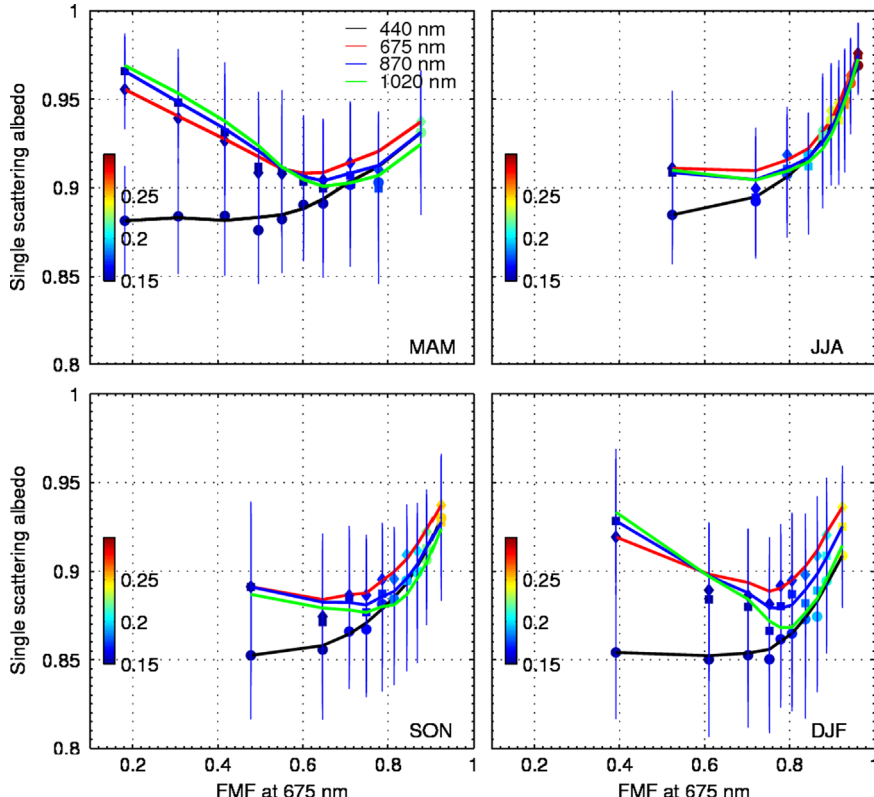


**Fig. 2.** Spectral single scattering albedo as a function of the fine mode fraction of aerosol optical depth (AOD) at 675 nm in the North China Plain (NCP). Dots and vertical lines represent the average and standard of single scattering albedo of each bin. Solid curve represent 5-point moving average. The color of dots represents the value of effective radius of fine mode aerosol.

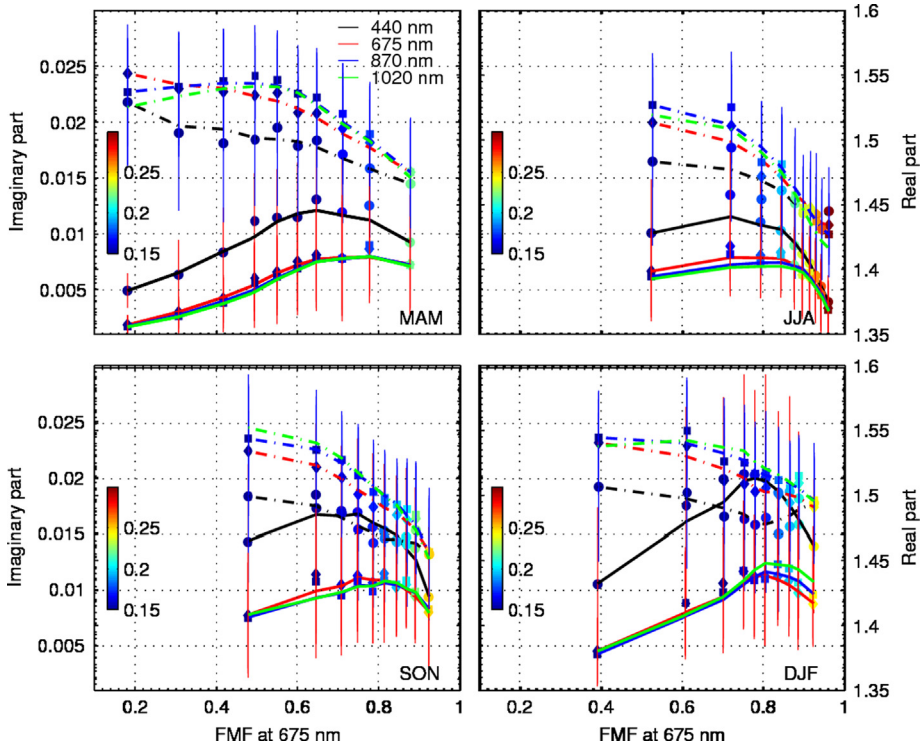


**Fig. 3.** Similar as figure but for spectral real (dashed line) and imaginary parts (solid line) of the refractive index as a function of the fine mode fraction of aerosol optical depth (AOD) at 675 nm in the North China Plain (NCP).

which likely occurred because  $\omega_{440\text{ nm}}$  of fine particles is larger than that of coarse particles [25]. When  $FMF$  exceeded 0.80,  $\omega$  increased rapidly in every season because  $RE_f$  and thereby aerosol scattering efficiency increased. An increase in  $RE_f$  was likely due to the hygroscopic growth or aerosol modification by fog or clouds [26], which was in good accordance with the observation such that the real and imaginary parts of the refractive index decreased with  $FMF$  and  $RE_f$  when  $FMF$  was  $>\sim 0.8$ .

### 3.2. Aerosol absorption/size and implications for aerosol classification

The best separation among aerosol type clusters can be achieved on the basis of a scatter-plot of the extinction Ångström exponent ( $EAE$ ) and  $\omega_{440\text{ nm}}$  [27]. Analysis of aerosol optical properties in a few representative AERONET sites showed that dust is characterized by an  $EAE$  of  $\sim 0.2\text{--}0.3$  and  $\omega_{440\text{ nm}}$  of  $\sim 0.89\text{--}0.93$ . The mixed aerosol category shows two primary density clusters with  $EAE$ s that differs significantly including  $\sim 0.4$  for mixed-large particles and  $\sim 1.25$  for mixed-small particles. The urban/industrial aerosol type is composed of small sub-micron particles ( $EAE\sim 1.65$ ) with weak absorption ( $\omega_{440\text{ nm}}\sim 0.95$ ). Biomass-burning aerosol has the largest  $EAE$  at  $\sim 1.95$  and  $\omega_{440\text{ nm}}$  that varies from 0.87 to 0.93 [27].

Fig. 4 presents the relative number density plots of seasonal  $EAE$  and  $\omega_{440\text{ nm}}$ . The primary density clusters are denoted by orange and red regions representing relative value levels of  $\sim 45\text{--}64$ . The first interesting feature is that

the dust category ( $EAE \sim 0.2\text{--}0.3$ ) occurred in all seasons, although 79% of cases were observed in spring. The overall mean  $\omega$  for the dust category ( $EAE < 0.20$ ) was 0.88, 0.95, 0.96, and 0.97 at 440, 675, 870, and 1020 nm, respectively, which were lower than that of pure dust [27], indicating possible incursions by carbonaceous particles. With the exception of dust cases, the average  $EAE$ ,  $\omega$ , and its spectra resembled that of the mixed category ( $0.6 < EAE < 1.5$  and  $\omega_{440\text{ nm}}\sim 0.82\text{--}0.93$ ) in every season except summer.  $EAE$  of the primary density clusters in spring varied from  $\sim 0.6$  to 1.3, and  $\omega_{440\text{ nm}}$  showed little variation. On the contrary,  $EAE$  remained stable, but  $\omega_{440\text{ nm}}$  varied from 0.82 to 0.92 in winter. Both  $EAE$  and  $\omega_{440\text{ nm}}$  of the primary density clusters in fall were stable ( $EAE \sim 1.1\text{--}1.4$ ;  $\omega_{440\text{ nm}}\sim 0.87\text{--}0.91$ ). In summer,  $\omega_{440\text{ nm}}$  at  $\sim 0.91\text{--}0.96$  was close to that for the industrial/urban aerosol category defined by Giles et al. [27], but the  $EAE$  was slightly lower at  $\sim 1.2\text{--}1.4$ . Variations in  $EAE$  and  $\omega_{440\text{ nm}}$  for the primary density clusters likely reflect variations in the sources and histories of air masses. Analysis of the dependence of  $\omega$  and  $EAE$  on the long-range transport of air masses in Beijing showed that both parameters when associated with slowly moving air masses were generally higher than those with fast moving air masses [13].

The absorption Ångström exponent (AAE) provides an indication of the dominance of carbonaceous particles or iron oxides in dust [28]. The average of AAE for the dust category was 1.98, which is slightly lower than that reported by Russell et al. [28]. As expected, relatively larger AAEs were observed in spring ( $1.51 \pm 0.47$ ) and winter ( $1.59 \pm 0.37$ ), likely due to

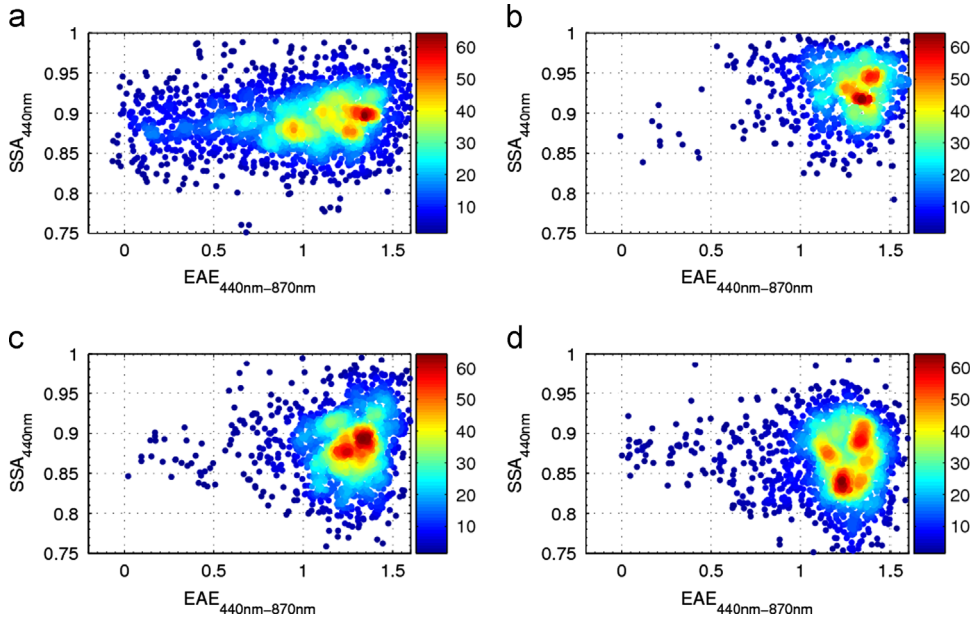


**Fig. 4.** Relative number density plots for the extinction Ångström exponent (440–870 nm) and single scattering albedo at 440 nm for the four seasons based on AERONET level 2.0 data. The color scale represents the relative density of points in each season, where orange to red colors (levels ~45–64) indicate the highest number density. (For interpretation of the references to color in this figure legend, the reader is referred to the web version of this article.)

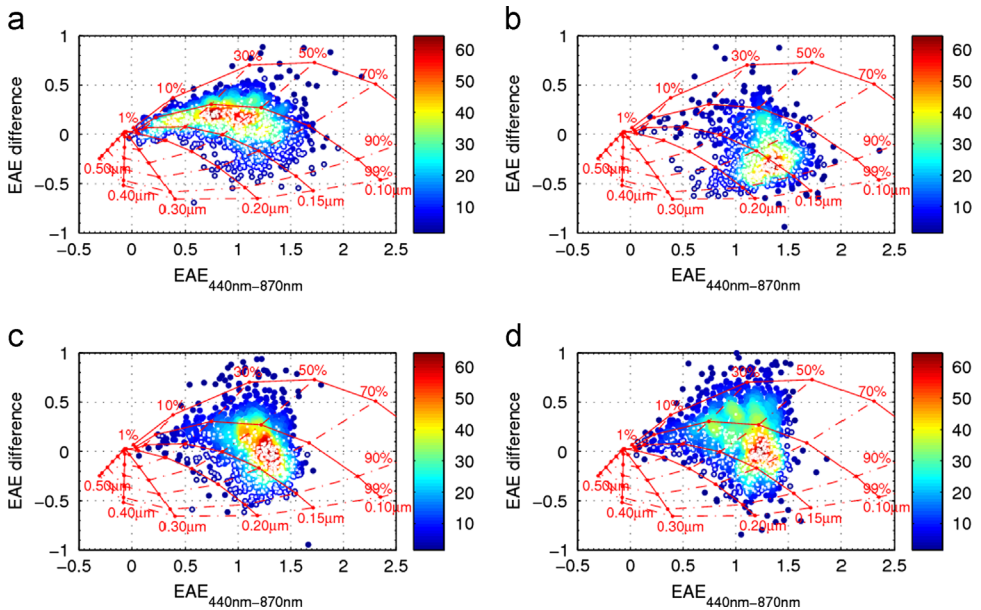


**Fig. 5.** Relative density plot of Ångström exponent (440–870 nm) and Ångström exponent difference (440–675 nm – 675–870 nm). White dots represent aerosol optical depth (AOD) at 440 nm is  $> 0.5$ .

the mixture of dust and anthropogenic aerosols in spring or the shell coating of larger optically effective BC particles ( $> 0.1 \mu\text{m}$ ) in winter.

EAE is a parameter reflecting the volume fraction of fine mode aerosols (radii  $< 0.6 \mu\text{m}$ ). The spectral difference of EAE wavelength pairs, here we use the difference between  $\text{EAE}_{440–675 \text{ nm}}$  and  $\text{EAE}_{675–870 \text{ nm}}$ , is a good indicator to fine mode effective radius [29,30]. Therefore, a

combination of these two parameters can be used to propose a graphical method for evaluating the concentration of fine mode particles to AOD and to track mixtures of pollution containing dust based on only AOD measurements at a few wavelengths [30]. Seasonal scatter plots of  $\text{EAE}$  and  $\text{EAE}$  difference ( $\text{EAE}_{440–675 \text{ nm}} – \text{EAE}_{675–870 \text{ nm}}$ ) are shown in Fig. 5. Some high AODs ( $> 0.5$ ) in Spring were characterized by lower  $RE_f$  (0.1–0.15) and  $FMF$  at 670 nm

(<30%) that reflected occasional dominant influence of dust aerosols [13]. However, the most outstanding feature in each season was that AOD growth generally remained associated to increasing  $RE_f$  and  $FMF$ . This feature suggests

that AOD growth is attributable to increasing concentration and size of fine model aerosols, i.e., AOD growth is mainly attributable to increasing anthropogenic emissions. This feature is more prominent in summer when the

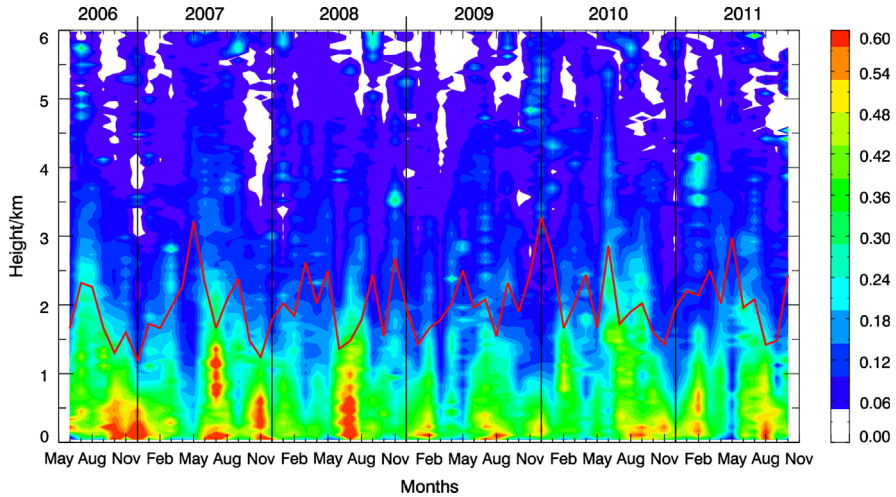


**Fig. 6.** Monthly all-sky nighttime profile of aerosol extinction coefficient ( $\text{km}^{-1}$ ) from July 2006 to October 2011 based on CALIOP version 3 Level 2 data.

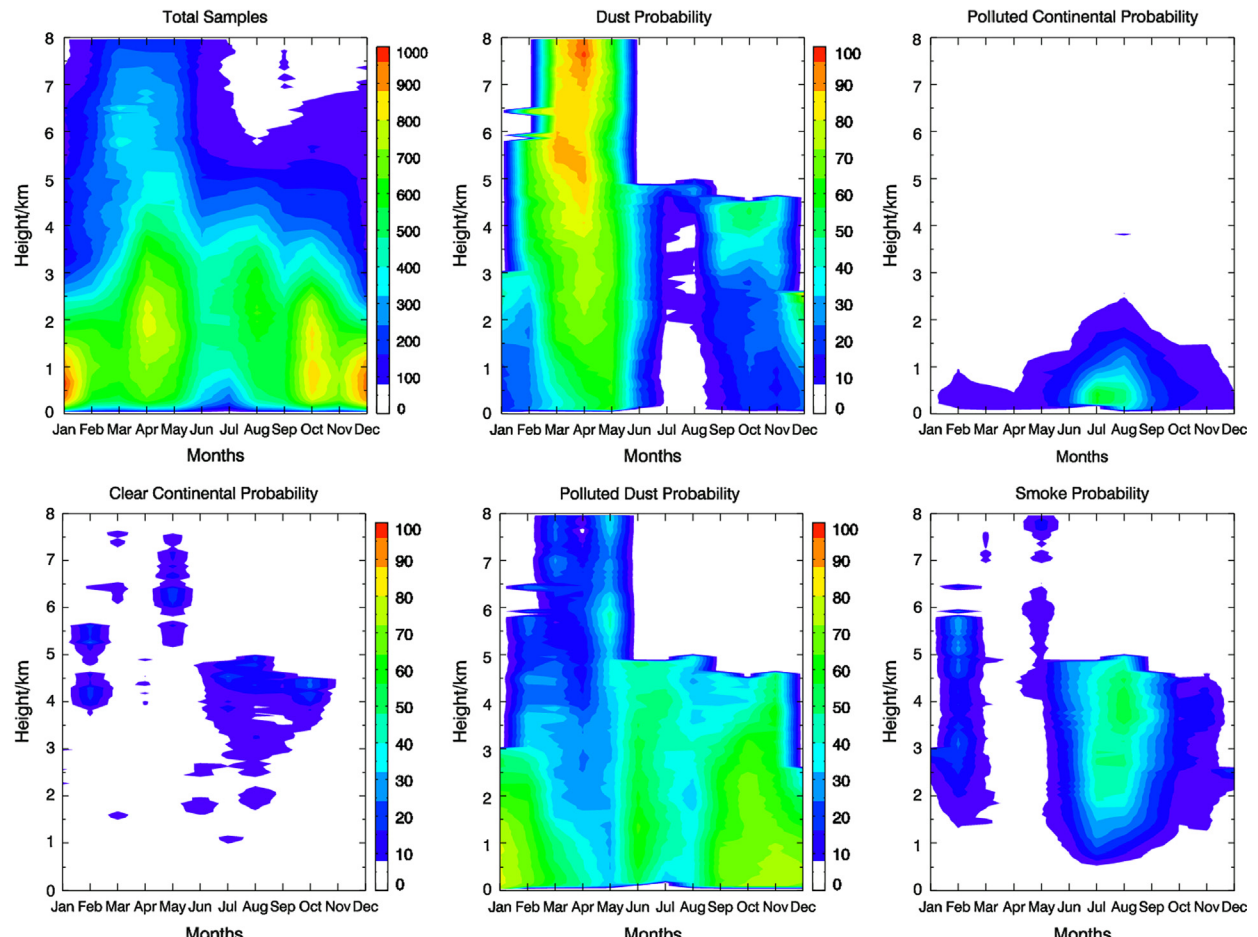


**Fig. 7.** Monthly profile of total observation number and occurrence of five major aerosol types defined in the CALIOP algorithm as dust, polluted continental, clear continental, polluted dust, and smoke.

largest  $RE_f$  and FMF has been observed. Remarkable increases in  $RE_f$  is likely due to the strongest hygroscopic growth or aerosol modification by fog and cloud processes in this rainy season [26].

### 3.3. Climatology of aerosol profile

The monthly nighttime average vertical profile (0.30–8.0 km altitude) of extinction coefficient at 532 nm from June 2006 to October 2011 over the NCP is shown in Fig. 6. Fig. 7 shows the occurrence frequency of the five major aerosol types. The extinction profile and occurrence of aerosol types showed pronounced seasonal and interannual variability. Strong convective activity resulted in an aerosol layer height of 2–3 km in summer; however, the aerosol layer was trapped below 1–2 km by subsidence in fall and winter. Although elevated mineral dust (up to 6 km) was often observed in spring, the aerosol layer remained below 1–2 km in spring. Polluted dust was the dominant aerosol type in the boundary layer, which is in accordance with the mixed category in AERONET data analysis. A high frequency of polluted dust (> 60%) was observed in June and from September to the following February. Elevated smoke was generally observed (> 1 km) from June to September. Analysis of MODIS active fire products revealed that fire activities often

occurred in May–June and in October–November, reflecting harvest seasons in the NCP. It appears that smoke aerosols are misidentified as polluted dust aerosols; likely because the volume depolarization ratio of smoke aerosols exceeds the threshold (0.075) used to separate smoke and polluted dust aerosols [24]. Polluted continental aerosols were observed mainly in the lower layer in summer when aerosols were classified as industrial/urban by the analysis of the AERONET data.

### 3.4. Evaluation of MODIS AOD retrievals

Fig. 8 presents the comparison results of MODIS level 2.0 AOD retrievals from Terra and Aqua satellites against AERONET observations. We employed the spatio-temporal technique to correlate satellite and ground observations [9], i.e., the AERONET AOT were averaged in time ( $\pm 0.5$  h of MODIS overpasses) and MODIS AOD data were averaged in space (over a  $5 \times 5$  array of 10 km pixels centered at each AERONET site). At least 2 out of 5 AERONET data points and 5 out of 25 MODIS pixels were required in the validation to minimize cloud contamination [9]. AOD generally was in good agreement; the correlation coefficients ranged from 0.86 to 0.96 with offsets of  $\sim 0.02$ – $0.08$ , slopes of  $\sim 0.76$ – $1.12$ , mean bias errors of  $\sim 0.03$ – $0.11$ , and relative bias of  $\sim 5$ – $34\%$ . Approximately 47–80% of retrievals were within the expected

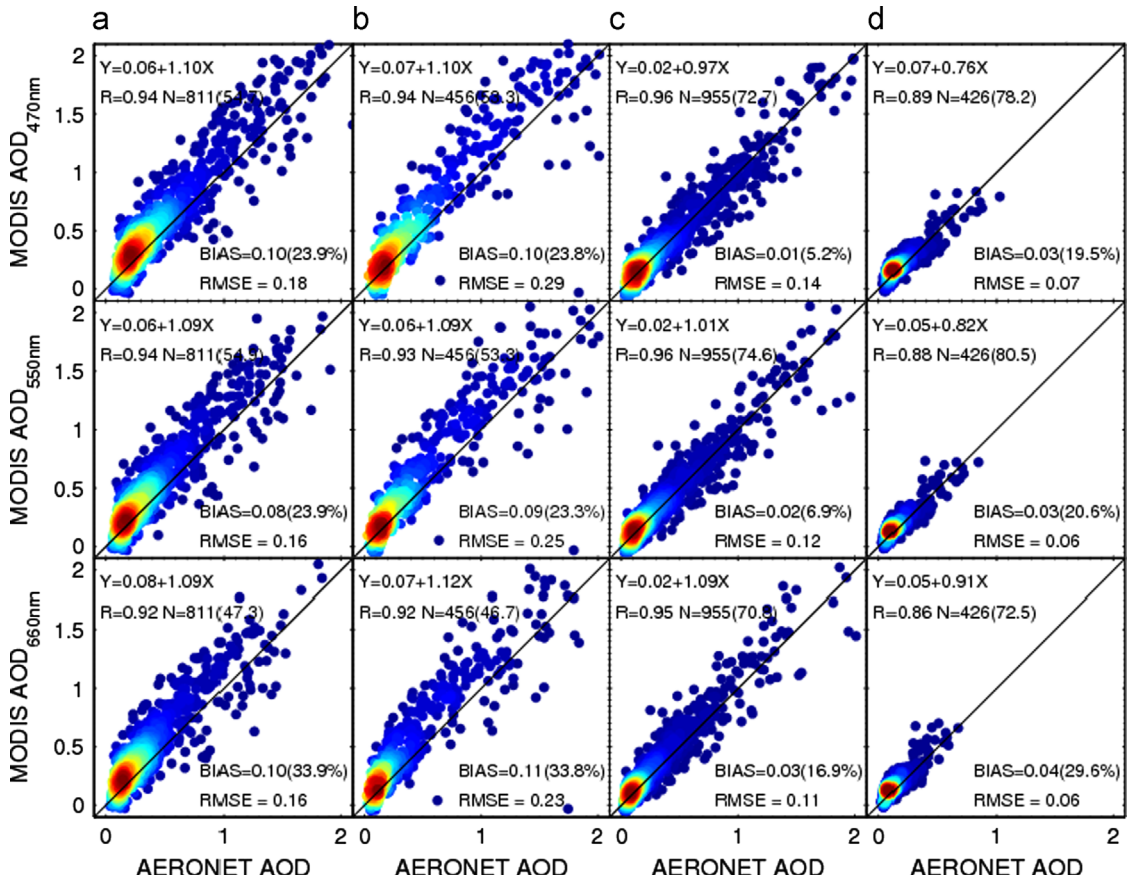


Fig. 8. Relative number density plots for the validation of MODIS aerosol optical depth (AOD) against AERONET AOD in the four seasons at 470 nm (upper), 550 nm (middle), and 675 nm (bottom). (a) MAM, (b) JJA, (c) SON and (d) DJF.

uncertainty envelop over land ( $\pm 0.05 \pm 0.20 \times \text{AOD}$ ). The best MODIS retrievals appeared in fall when aerosol optical properties were stable and were captured properly by the MODIS aerosol algorithm [15]. It should be noted that MODIS tended to overestimate AOD in every season; this feature was most prominent in spring and summer. A non-absorbing aerosol model should be suitable in summer, as shown in Figs. 2 and 3; however, a moderate absorbing aerosol model was adapted in the MODIS aerosol algorithm [15], which likely led to the MODIS overestimation. In spring, aerosols showed moderate absorption capability and were modeled properly by the MODIS aerosol algorithm. Nevertheless, the ratio of surface reflectance between 670 nm and 2100 nm was  $\sim 0.6$  in the NCP [9], which is slightly higher than that in the MODIS aerosol algorithm. This discrepancy is a likely cause for MODIS overestimation. Overestimation was more prominent at 670 nm than that at 470 nm, leading to poor estimations of EAE. The dust model generally provided the best fit to the MODIS reflectance; MODIS EAEs were generally close to 0.6. The selection of the dust model produced little effect on the AOD correlation over this region, where a significant amount of dust was expected; however, this selection obviously resulted in poor retrievals of aerosol size. Mielonen et al. suggested that the flawed aerosol model selection and resulting poor EAE retrieval was mainly caused by the improper surface reflectance assumption at 670 nm in the MODIS algorithm [31]. Given the fact that EAE is required

for estimating the anthropogenic component of aerosols over land, improvement of surface reflectance assumption and thereby the selection of aerosol model in the MODIS aerosol algorithm requires further study.

### 3.5. Spatial variation of AOD and climatology of regional aerosol pollution

Similar trends in aerosol concentration were often observed in the urban and surrounding areas of NCP. And aerosol pollution was often spatially uniform, indicating that the aerosol pollution was regional in nature [6,7]. This feature is clearly represented in Fig. 9, in which seasonal spatial distribution of Terra AOD overlain by the National Centers for Environmental Prediction reanalysis wind vector at 850 h Pa is shown. Spatially uniform aerosol pollution was often observed in the plain areas in every season [6,7,14]. More specifically, occasionally dust events sweep across NCP in dry and windy spring, leading to a regional mixture of coarse dust particles with anthropogenic pollution created by industrial and agricultural activities in NCP [13]. NCP is often covered by a thick layer of haze ( $\text{AOD} > 1.0$ ) in summer. Local air in NCP is influenced by aged air pollution that is transported by a slow southern wind. Transportation of aerosols and water vapor is bordered by the Yanshan Mountain toward the north and west, leading to smog pollution in NCP. The vast anticyclone high pressure system in fall takes hold and brings dry and

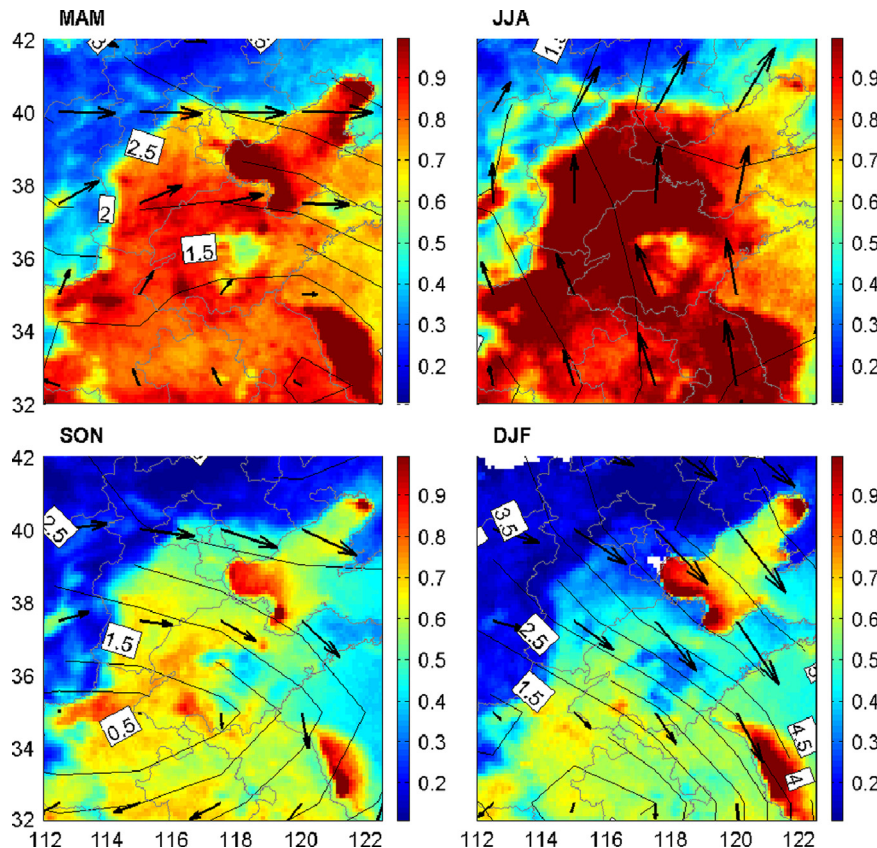


**Fig. 9.** Seasonal average Terra/MODIS aerosol optical depth (AOD) in the North China Plain (NCP) overlain by the seasonal average wind speed reported by the National Centers for Environmental Prediction.

clean air from north and west, leading to an abrupt cleanup of the haze in a matter of one day or less because of the passage of cold fronts [14]. In winter, the prevailing strong wind from the northwest brings clean air to the NCP, and polluted air is swept to the downwind region, resulting in relatively lower AODs ( $< 0.5$ ). Spatially uniform aerosol pollution was also supported by the spatial distribution of linear correlation coefficients between daily AERONET AODs at Beijing and Terra level 2.0 pixel AODs (Fig. 10). A strong correlation ( $R > 0.7$ ) persisted for large and strongly anisotropic areas covering  $\sim 17,000 \text{ km}^2$  in winter to  $\sim 100,000 \text{ km}^2$  in fall. The zone with larger  $R$  generally extended in a southwesterly direction from the polluted areas to relatively clean areas in the northeast. The boundary layer height in winter was relatively lower, which likely prohibited the regional mixture of aerosol pollution and thereby resulted in small areas of  $R > 0.7$ . In spring, a several large correlation coefficients were also observed in areas of northwest of Beijing, indicating that spring AOD in that region was impacted by dust aerosols via long-range transportation [13].

### 3.6. Variability and trends of AOD

Knowledge of variability and long-term trends of aerosol optical properties is required for better understanding of climate changes [32]. Detection of such trends is important for climate studies of remote sensing data

because limited long-term observations carry uncertainties [33]. Surface and satellite remote sensing data recorded during the past decade in the Beijing area provide an opportunity to study AOD changes and to determine whether similar trends can be detected from ground and satellite retrievals. To minimize the effects of the magnitude of variability and autocorrelation of the noise contained in the data, we adopted a statistical procedure to estimate the trends by fitting the following statistical model for monthly AOD with a least mean squares (LMS) approximation [34]:

$$\text{AOD}_t = m + C_t + \rho(t/12) + M_t,$$

where  $m$  is a constant term,  $C_t$  is a seasonal component, and  $\rho$  is the magnitude of the trend per year.  $M_t$  is the unexplained portion of the data, which is assumed to be an [AR(1)] process. An actual trend is indicated at the 95% confidence level if  $|\rho/\sigma_\rho| > 2$ , where  $\sigma_\rho$  is the standard deviation of the slope. Daily MODIS AODs were averaged over pixel arrays of  $0.5 \times 0.5^\circ$ ,  $1.0 \times 1.0^\circ$ , and  $2.0 \times 2.0^\circ$  at the Beijing AERONET site. Additionally, daily MODIS AODs were averaged over pixels with  $R > 0.7$  in the NCP. Fig. 11 presents the monthly mean and deviation of AODs derived from AERONET and Terra (upper panel) and from AERONET and Aqua (bottom panel). A clear seasonality as well as a large interannual variation of AOD is clearly indicated by the ground and satellite retrievals. AOD showed large oscillation over the past decade. AODs before the mid-2003 were

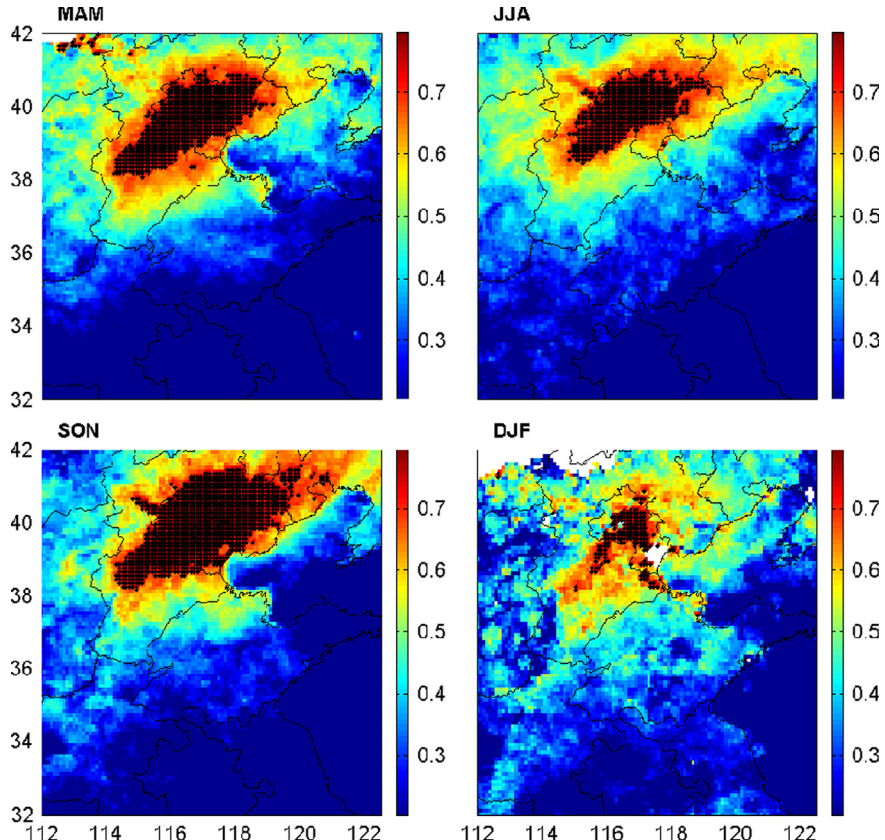


**Fig. 10.** Spatial distribution of the correlation coefficients between daily AERONET aerosol optical depth (AOD) in Beijing and Terra MODIS Level 2 pixel AOD in the four seasons. The black dot indicates coefficients  $> 0.7$ .

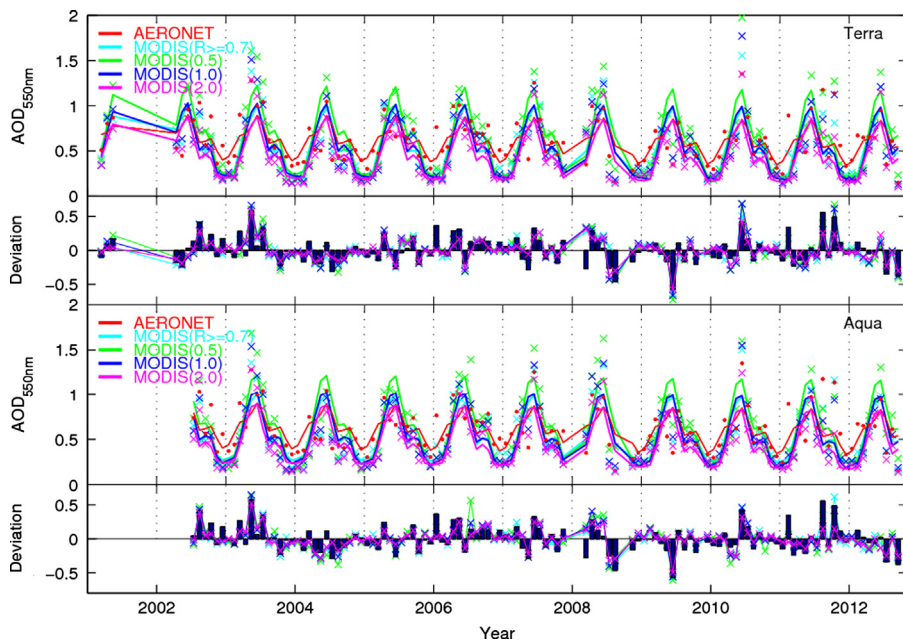


**Fig. 11.** Monthly average and deviation of AERONET aerosol optical depth (AOD) and MODIS AOD and their least mean square (LMS) fits (solid line).

**Table 2**

Least mean squares (LMS) aerosol optical depth (AOD) trend derived from AERONET data at Beijing and Terra MODIS.  $\rho$  is the trend and  $\sigma_\rho$  is the standard deviation of the trend. NY is the number of years required for detecting a significant trend.

AERONET (March 2000–June 2012)				Terra MODIS				
$\rho$ ( $\text{yr}^{-1}$ )	$\rho$ ( $\% \text{yr}^{-1}$ )	$\rho/\sigma_\rho$	NY	Area	$\rho$ ( $\text{yr}^{-1}$ )	$\rho$ ( $\% \text{yr}^{-1}$ )	$\rho/\sigma_\rho$	NY
-0.0062	-1.13	-1.02	24	$R > 0.7$	-0.0043	-1.07	-0.77	24
				$0.5 \times 0.5$	-0.0065	-1.33	-1.02	21
				$1.0 \times 1.0$	-0.0045	-1.04	-0.85	25
				$2.0 \times 2.0$	-0.0056	-1.58	-1.23	19

**Table 3**

Similar as Table 2 but for AERONET data at Beijing and Aqua MODIS.

AERONET (June 2002–June 2012)				Aqua MODIS				
$\rho$ ( $\text{yr}^{-1}$ )	$\rho$ ( $\% \text{yr}^{-1}$ )	$\rho/\rho_\sigma$	NY	Area	$\rho$ ( $\text{yr}^{-1}$ )	$\rho$ ( $\% \text{yr}^{-1}$ )	$\rho/\rho_\sigma$	NY
-0.0079	-1.15	-1.29	20	$R > 0.7$	-0.0037	-0.69	-0.67	29
				$0.5 \times 0.5$	-0.0064	-1.20	-1.02	20
				$1.0 \times 1.0$	-0.0062	-1.20	-1.14	20
				$2.0 \times 2.0$	-0.0082	-1.95	-1.80	14

generally larger than the decadal average. Nevertheless, negative deviations were observed in 2004, and AODs have increased gradually from 2004 to 2008. Satellite retrievals of air pollutants such as  $\text{NO}_2$  by the Ozone Monitoring Instrument and AOD by the Multi-angle Imaging Spectroradiometer and the Polarization and Anisotropy of Reflectances for Atmospheric Sciences also showed an increase in air pollution during 2004–2008 in the NCP [35,36]. AOD decreased from August 2008 to the end of 2009, which is likely associated with air pollution control measurements taken for the Beijing Olympic Games in 2008 and economic

crises in 2009 [36]. Atmospheric pollution emission sources should not vary dramatically at the interannual scale, excluding significant temporary effects on air pollution by several voluntary and involuntary socioeconomic events. Therefore, large interannual AOD variations should be closely related to changes in the synoptic system and atmospheric circulation, which requires further study. A decreasing trend was derived for AERONET and MODIS AOD time series during the new century, although no trends were significant (Tables 2 and 3). Confidence of this analysis could be improved by observing the consistency between trends derived from these datasets.

It is estimated that observations of more than 20 years are required to detect a significant trend; therefore, long-term ground and satellite observations of aerosol optical properties should be maintained.

#### 4. Conclusion

Heavy anthropogenic pollutions from urbanization, industrial, and agricultural activities mixed with coarse dust particles resulted in a rather complex nature of aerosol physical and optical properties in the NCP. Analysis of ground and satellite remote sensing aerosol optical data recorded during the past decade showed distinct seasonal and interannual variation of aerosol optical properties.

The effective radius of fine mode component was stable when *FMF* was  $<\sim 0.6\text{--}0.7$ , and the external linear mixing of both fine and coarse mode components dominated variations of the refractive index, and thereby  $\omega$ , in spring and winter. The effective radius of the fine mode component increased rapidly with *FMF* due to hygroscopic growth or fog- and cloud-induced aerosol modification when *FMF* exceeded  $\sim 0.6\text{--}0.7$ , which resulted in dramatic increase in  $\omega$ . With the exception of dust cases, the average *EAE*,  $\omega$ , and its spectra resembled that of the mixed category in every season except summer. Summer aerosol resembled the industry/urban category but showed relatively smaller *EAE* values of 1.2–1.4 versus 1.6. Strong convective activity led to an atmospheric pollution layer of 2–3 km in summer. Trapping of pollution at low altitudes below 1–2 km by subsidence occurred in fall and winter.

MODIS AOD was in good agreement with AERONET data ( $R > 0.80$ ). MODIS tended to overestimate AOD in spring and summer, occurring most prominently at 660 nm. Surface reflectance parameterization, and thereby the selection of aerosol model, in the MODIS aerosol algorithm requires further study to improve MODIS AOD and EAE retrievals. A strong correlation ( $R > 0.7$ ) between AEROENT AOD in Beijing and MODIS Level 2.0 pixel AODs persisted for large and strongly anisotropic areas of  $\sim 17,000 \text{ km}^2$  in winter to  $\sim 100,000 \text{ km}^2$  in fall, indicating regional pollution in the NCP. Distinct seasonality and large interannual variation of AOD was observed by AERONET and MODIS. Decreasing trends were derived for the AERONET and MODIS AOD time series, although all trends were not significant. It was estimated that observations with more than 20 years were required to detect a significant trend.

#### Acknowledgments

This research was supported by the Strategic Priority Research Program of the Chinese Academy of Sciences (Grant no. XDA05100301) and the National Science Foundation of China (Grant no. 41175031). The satellite data were obtained from the Atmospheric Science Data Center.

#### References

- [1] Gunnar M. Consistency between satellite-derived and modeled estimates of the direct aerosol effect. *Science* 2009;325:187–90.
- [2] Tao W, Chen J, Li Z, Wang C, Zhang C. Impact of aerosols on convective clouds and precipitation. *Rev Geophys* 2012; <http://dx.doi.org/10.1029/2001RG000369>, in press.
- [3] Qiu J, Yang L. Variation characteristics of atmospheric aerosol optical depths and visibility in North China during 1980–1994. *Atmos Environ* 2000;34:603–9.
- [4] Luo Y, Lu D, Zhou X, Li W, He Q. Characteristics of the spatial distribution and yearly variation of aerosol optical depth over China in last 30 years. *J Geophys Res* 2001;106:D14501–13.
- [5] Xia X, Chen H, Goloub P, Zhang W, Chatenet B, Wang P. A compilation of aerosol optical properties and calculation of direct radiative forcing over an urban region in northern China. *J Geophys Res* 2007;112:D12203. <http://dx.doi.org/10.1029/2006JD008119>.
- [6] Li Z, Chan H, Cribb M, Dickerson R, Holben B, Li C, et al. Preface to special section on East Asian Studies of Tropospheric Aerosols: an International Regional Experiment (EAST-AIRE). *J. Geophys. Res.* 2007;112:D22S00. <http://dx.doi.org/10.1029/2007JD008853>.
- [7] Li Z, Li C, Chen H, Tsay S, Holben B, Huang J, et al. East Asian studies of tropospheric aerosols and their impact on regional climate (EAST-AIRE): an overview. *J Geophys Res* 2011;116:D00K34. <http://dx.doi.org/10.1029/2010JD015257>.
- [8] Eck T, Holben B, Sinyuk A, Pinker R, Goloub P, Chen H, et al. Climatological aspects of the optical properties of fine/coarse mode aerosol mixtures. *J Geophys Res* 2010;115:D19205, <http://dx.doi.org/10.1029/2010JD014002>.
- [9] Li Z, Niu F, Lee K-H, Xin J, Hao W-M, Nordgren B, et al. Validation and understanding of Moderate Resolution Imaging Spectroradiometer aerosol products (C5) using ground-based measurements from the handheld Sun photometer network in China. *J Geophys Res* 2007;112:D22S07. <http://dx.doi.org/10.1029/2007JD008479>.
- [10] Xia X. Significant overestimation of aerosol optical thickness by MODIS over global land. *Chinese Sci Bull* 2006;51(23):2905–12.
- [11] Xia X, Chen H, Li Z, Wang P, Wang J. Significant reduction of surface solar irradiance induced by aerosols in a suburban region in north-eastern China. *J Geophys Res* 2007;112:D22S02. <http://dx.doi.org/10.1029/2006JD007562>.
- [12] Liu J, Xia X, Wang P, Li Z, Zheng Y, Cribb M, et al. Significant aerosol direct radiative effects during a pollution episode in northern China. *Geophys Res Letts* 2007;34:L23808. <http://dx.doi.org/10.1029/2007GL030953>.
- [13] Xia X, Chen H, Zhang W. Analysis of the dependence of column-integrated aerosol properties on long-range transport of air masses in Beijing. *Atmos Environ* 2007;41:7739–50.
- [14] Li Z, Xia X, Cribb M, Mi W, Holben B, Wang P, et al. Aerosol optical properties and their radiative effects in northern China. *J Geophys Res* 2007;112:D22S01. <http://dx.doi.org/10.1029/2006JD007382>.
- [15] Levy R, Remer A, Kleidman R, Mattoo S, Ichoku C, Kahn R, et al. Global evaluation of the collection 5 MODIS dark-target aerosol products over land. *Atmos Chem Phys* 2010;10:10399–420.
- [16] Li C, Mao J, Lau K, Chen J, Yuan Z, Liu X, et al. Characteristics of distribution and seasonal variation of aerosol optical depth in eastern China with MODIS products. *Chin Sci Bull* 2003;48:2489–95.
- [17] He Q, Li C, Geng F, Lei Y, Li Y. Study on long-term aerosol distribution over the land of east china using MODIS data. *Aero Air Qual Res* 2012;12:304–19.
- [18] Kaufman YJ, Koren I, Remer LA, Rosenfeld D, Rudich Y. The effect of smoke, dust and pollution aerosol on shallow cloud development over the Atlantic Ocean. *Proc Natl Acad Sci USA* 2005;102(32):11,207–12.
- [19] Yu H, Remer LA, Chin M, Bian H, Kleidman RG, Diehl T. A satellite-based assessment of transpacific transport of pollution aerosols. *J Geophys Res* 2008;113:D14S12. <http://dx.doi.org/10.1029/2007JD009349>.
- [20] Dubovik O, Lapyonok T, Kaufman YJ, Chin M, Ginoux P, Kahn R, et al. Retrieving global sources of aerosols from satellites using inverse modeling. *Atmos Chem Phys* 2008;8:209–50.
- [21] Winker D, Tackett J, Getzewich B, Liu Z, Vaughan M, Rogers R, et al. The global 3-D distribution of tropospheric aerosols as characterized by CALIOP. *Atmos Chem Phys* 2013;13:3345–61, <http://dx.doi.org/10.5194/acp-13-3345-2013>.
- [22] Holben BN, Tanre D, Simirnov A, Eck T, Slutsker I, Abuhassan N, et al. An emerging ground-based aerosol climatology: aerosol optical depth from AERONET. *J Geophys Res* 2001;106(D11):12,067–97. <http://dx.doi.org/10.1029/2001JD900014>.
- [23] Dubovik O, Sinyuk A, Lapyonok T, Holben B, Mishchenko M, Yang P, et al. Application of spheroid models to account for aerosol particle nonsphericity in remote sensing of desert dust. *J Geophys Res* 2006;111:D11208. <http://dx.doi.org/10.1029/2005JD006619>.

- [24] Omar A, Winker D, Vaughan M, Hu Y, Trepte C, Ferrare R, et al. The CALIPSO automated aerosol classification and lidar ratio selection algorithm. *J Atmos Ocean Tech* 2009;26:1994–2014.
- [25] Yang M, Howell S, Zhuang J, Huebert B. Attribution of aerosol light absorption to black carbon, brown carbon, and dust in China—interpretations of atmospheric measurements during EAST-AIRE. *Atmos Chem Phys* 2009;9:2035–50.
- [26] Eck TF, Holben B, Reid J, Giles D, Rivas M, Singh R, et al. Fog- and cloud-induced aerosol modification observed by the Aerosol Robotic Network (AERONET). *J Geophys Res* 2012;117:D07206. <http://dx.doi.org/10.1029/2011JD016839>.
- [27] Giles D, Holben B, Eck T, Sinyuk A, Smirnov A, Slutsker I, et al. An analysis of AERONET aerosol absorption properties and classifications representative of aerosol source regions. *J Geophys Res* 2012;117:D17203. <http://dx.doi.org/10.1029/2012JD018127>.
- [28] Russell P, Bergstrom R, Shinozuka Y, Clarke A, DeCarlo P, Jimenez J, et al. Absorption Angstrom Exponent in AERONET and related data as an indicator of aerosol composition. *Atmos Chem Phys* 2010;10: 1155–69. <http://dx.doi.org/10.5194/acp-10-1155-2010>.
- [29] Gobbi GP, Kaufman YJ, Koren I, Eck TF. Classification of aerosol properties derived from AERONET direct sun data. *Atmos Chem Phys* 2007;7:453–8. <http://dx.doi.org/10.5194/acp-7-453-2007>.
- [30] Che H, Yang Z, Zhu X, Ma C, Zhou Q, Wang P. Study on the aerosol optical properties and their relationship with aerosol chemical compositions over three regional background stations in China. *Atmos Environ* 2009;43:1093–9.
- [31] Mielonen T, Levy R, Aaltonen V, Komppula M, Leeuw G, Huttunen J, et al. Evaluation the assumptions of surface reflectance and aerosol type selection within the MODIS aerosol retrieval over land: the problem of dust type selection. *Atmos Meas Tech* 2011;4:201–14.
- [32] Mishchenko M, Geogdzhayev I, Rossow W, Cairns B, Carlson B, Lacis A, et al. Long-term satellite record reveals likely recent aerosol trend. *Science* 2007;315:1543.
- [33] Mishchenko M, Geogdzhayev I, Cairns B, Carlson B, Chowdhary J, Lacis A, et al. Past, present, and future of global climatologies derived from satellite observations: a perspective. *J Quant Spectrosc Radiat Transfer* 2007;106:325–47.
- [34] Weatherhead E, Reinsel G, Tiao G, Ment X, Choi D, Cheang W, et al. Factors affecting the detection of trends: statistical considerations and applications to environmental data. *J Geophys Res* 1998;103: 17149–61.
- [35] Su X, Goloub P, Chiapello I, Chen H, Ducos F, Li Z. Aerosol variability over East Asia as seen by POLDER space-borne sensors. *J Geophys Res* 2010;. <http://dx.doi.org/10.1029/2010JD014285>.
- [36] Lin J, Pan D, Zhang R. Trend and interannual variability of Chinese air pollution since 2000 in association with socioeconomic development: a brief overview. *Atmos Ocean Sci Lett* 2013;6:84–9.